

Size Effect on Flexural Compressive Strength of Reinforced Concrete Flexural Members

J.K. Kim

Korea Advanced Institute of Science and Technology, Taejon, Korea.

S.T. Yi

Chung Cheong University, Cheongwon, Chungbuk, Korea.

J.J.H. Kim

Sejong University, Seoul, Korea.

K.M. Lee

Sungkyunkwan University, Suwon, Korea.

ABSTRACT: It is important to consider the effect of member size when estimating the ultimate strength of a concrete flexural member because the strength always decreases with an increase of member size. In this study, the size effect of a reinforced concrete (RC) beam was experimentally investigated. For this purpose, a series of beam specimens subjected to four-point loading were tested. More specifically, three different effective depth ($d=15, 30,$ and 60 cm) RC beams were tested to investigate the size effect. The shear-span to depth ratio ($a/d=3.0$) and the thickness ($b=20$ cm) of the specimens were kept constant. Where the size effect in out-of-plane direction is not considered. The test results are curve fitted using Levenberg-Marquardt's Least Square Method (LSM) to obtain parameters for Modified Size Effect Law (MSEL) by Kim and Eo. The analysis results show that the flexural compression strength and ultimate strain decrease as the specimen size increases. Finally, parameters for MSEL are newly suggested. They also show that the current strength criteria-based design practice should be reviewed to include member size effect. More studies are needed in the future to verify that.

Keywords: size effect; flexural member; flexural compressive strength; stress-strain relationship; modified size effect law (MSEL).

1 INSTRUCTION

Currently, researchers in the field accept the conclusion that the failure of concrete loaded in tension is caused by strain localization resulting in a finite size fracture process zone. In the last few years, many researchers have begun to realize that strain localization also occurs for concrete specimens loaded in compression.^{1,2} However, the compressive failure mechanism is more complex than the tensile failure mechanism. Size effect of compressive failure is not as distinct as in tensile failure, because the formation of microcracks in compressive failure is distributed in a wider region than in tensile failure. Presently, most design codes for concrete structures do not consider the effect of size.

Concrete is a construction material normally used to withstand compressive force. However, specimens loaded in tension and compression both fail by the formation of distributed splitting cracks in the direction of member length as the lateral deformation increases. Thus, it is logical to extend

the tensile size effect research to compressive failure research. For this reason, several researchers are currently performing many studies on compressive failure of concrete. Gonnerman³ experimentally showed that the ratio of the compressive failure stress to the compressive strength decreases as the specimen size increases.

After deriving Size Effect Law (SEL) by Bazant,⁴ Kim et al.^{5,6} proposed the modified size effect law (MSEL, Eq. (1) by adding the size independent strength $\sigma_o (= \alpha f'_c)$ to SEL that can predict the strength of concrete members with or without initial cracks and with similar or dissimilar cracks.

$$\sigma_N = \frac{Bf'_c}{\sqrt{1 + \frac{D}{\lambda_o d_a}}} + \alpha f'_c \quad (1)$$

where, σ_N is the nominal strength; f'_c is the compressive strength of standard cylinder; D is the characteristic dimension; d_a is the maximum aggregate size; and B , λ_o , and α are empirical constants. As an application of MSEL, some

researches⁷⁻¹⁰ have been performed on unnotched and notched cylindrical specimens subjected to uniaxial compressive force, axially loaded Double Cantilever Beam, and C-shaped specimens subjected to flexural compression force. In Equation 1, the width of crack band l_o is empirically found to be related to the maximum aggregate size, e.g., $l_o = \lambda_o d_a$ in which λ_o is an approximate constant with values between of 2.0 and 3.0.⁷⁻⁹ In the regression analysis, this constant is selected as 2.0 where $l_o = 2.0 \times d_a = 4.0$ cm.

The actual stress distribution in the compression zone of reinforced concrete (RC) flexural members is extremely difficult to measure and to adequately model. In 1955, Hognestad et al.¹¹ experimentally presented concrete stress distribution in an ultimate strength design by a rising curve from zero to maximum stress, and a descending curve beyond the maximum stress. The test procedure on C-shaped concrete specimens subjected to axial load and bending moment was developed by the Portland Cement Association (PCA)^{11,12} at this time formed the basis of the rectangular stress block used in ACI 318 Code.¹² Also, Kim et al.'s studies⁸⁻¹⁰ have shown that under flexural compression loading the failure strengths decrease as the sizes (that is, size, length, and depth variations) of the concrete specimens increase. Since the most widely used flexural member type is RC beams, it is logical extend the study of flexural compressive strength size effect to flexural loaded beam members. Presently, however, both experimental and analytical studies considering the depth of neutral axis for RC beam specimens are scarce to the point of nonexistence due to numerous difficulties experimentally in measuring the stress-strain distribution.

The purpose of this study is to experimentally investigate the size dependency on flexural compressive strength, which is flexural strength of RC beams, considering the depth of neutral axis. Previously, several researchers have reported from their studies that flexural compressive strength size effect does not exist. However, the analyses show that the specimens used for the study had limited size variation and the neutral axis depth variations were too similar to show distinct size effect. Therefore, this study enforced distinct neutral axis depth variations for all of the tested specimens. Also, analytical equations that reasonably predict the size effect of flexural compressive strength are proposed based on the experimental data obtained from the flexural tests of RC beam specimens, which is designed and constructed in the actual field.

2 TEST SPECIMENS AND EXPERIMENTAL PROGRAM

2.1 Test specimens

The dimensions, shape, loading point locations, specimen number, and reinforcement details of specimens used in the experiments are shown in Figure 1 and Table 1. The main test variable was effective depth of the specimen ($d = 15, 30,$ and 60 cm), with the same concrete compressive strength of 37 MPa. The shear-span to depth ratio ($a/d = 3.0$) and the thickness ($b = 20$ cm) was kept constant so that the effect of thickness of specimen on the size effect can be eliminated. The central section of beam, the critical section under flexural compression loading, was not reinforced with shear reinforcement. The reinforcement, as shown in Figure 1, was used at the two ends of the specimen to eliminate the shear failure at the two end sections.

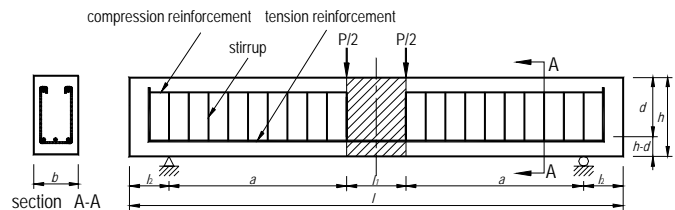


Figure 1. Shape and dimensions of specimens.

Table 1. Specimen size and reinforcement details.

Specimen No.	I	II	III
h (cm)	65	35	20
d (cm)	58.5	30.0	14.3
l_1 (cm)	60	30	15
l (cm)	460	230	125
a (cm)	180	90	45
l_2 (cm)	20	20	20
Tensile reinforcement	2-D25+D19	2-D16+D19	3-D13
Compressive reinforcement	2-D10	2-D10	2-D10
Stirrup	D10@200	D8@100	D6@50
Tensile reinforcement ratio (ρ_t) (%)	1.11	1.14	1.33
ρ_t /balanced reinforcement ratio	0.45	0.44	0.42

According to Table 1, tensile reinforcement ratios are different for different specimen sizes. The difference is to consider slight variations of yield strengths for various reinforcing bar diameters as shown in Table 2. In this experiment, tensile reinforcement ratios were adjusted to represent the same failure behavior for all

specimens at the time of yielding of reinforcing bars.

Table 2. Test results of reinforcing bar.

	Yield strength, f_y (MPa)	Ultimate strength, f_u (MPa)	f_u/f_y
D13	390.83	582.32	1.49
D16	445.28	666.30	1.50
D19	473.23	693.27	1.46
D25	467.55	697.10	1.49

The concrete mixture proportions selected for the beam and 28-day compressive strength cylinder specimens are listed in Table 3. The design strength and slump are 35 MPa and 12 cm, respectively. Type I portland cement was used in all mixtures. Crushed gravel is used as the coarse aggregate and the maximum aggregate size d_a is 20 mm. As listed in Table 3, concrete compressive strength f'_c , splitting tensile strength f_{ct} , and elastic modulus E_c are averaged values from testing of three identical ϕ 100×200 mm cylinders in the series. Specimens are cast vertically on a level surface. Two specimens, totally 6 specimens, per specimen size are prepared. All beam specimens and cylinders were removed from the mold after 24 hours and dry-cured under a wet burlap/tower until testing. The cylinders were tested at an age similar to the concrete used for the beam specimens.

Table 3. Concrete mixture proportions and physical properties of concrete.

w/c*	s/a**	Unit weight, kg/m ³				MPa		
%	%	W	C	S	G***	f'_c	f_{ct}	E_c
45	41	186	409	643	1017	37	4	27700

Table 4. Test results of beam specimens.

Specimen No.	σ_N (MPa)	P_u (kN)	$\epsilon_{u,test}$ ($\times 10^{-6}$)	$\epsilon_{u,anal}$ ($\times 10^{-6}$)
I-1	37.57	486.58	2200	2825
I-2	36.10	479.71	2270	2720
II-1	39.73	247.21	3080	3245
II-2	40.42	243.29	2990	3130
III-1	43.46	128.51	3370	4110
III-2	42.67	126.55	3410	4420

The numbering of the specimen (that is, I-1) and experimental data are tabulated in Table 4. Also, the roman numerals I, II, and III represent the size of the specimens with I being the largest and

decreasing accordingly. The arabic numbers 1 and 2 are the two specimens tested for each specimen size.

2.2 Experimental program

The applied loads in four-point loading shown in Figure 1 was supplied by a universal testing machine (UTM) with a capacity of 2500 kN using a displacement control method. During testing, loads were measured up to failure by load cells. The horizontal thick solid lines in Figure 2 represent the locations where strain gages are attached to the sides of specimens. As shown in Figure 2 and Table 5, strains were measured using 11, 11, and 9 strain gages attached to each side of specimen I, II, and III, correspondingly. The strain gages in the compression zone were attached more closely than the tension zone. In addition, 8, 6, and 6 linear variable displacement transducers (LVDTs) were used to monitor vertical displacements at each side of specimen I, II, and III, correspondingly.

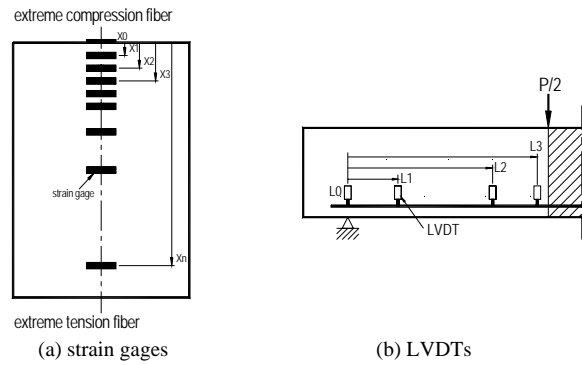


Figure 2. Locations of strain gages and LVDTs.

Table 5. Locations of strain gages and LVDTs.

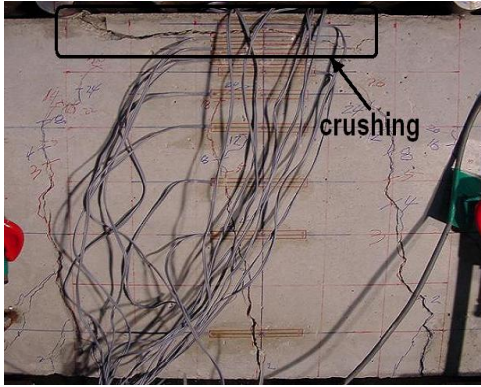
Xi (cm)		0, 2, 4, 6, 8, 10, 14, 20, 30, 40
strain gage	I	0, 2, 4, 6, 8, 10, 14, 20, 30, 40
	II	0, 1, 2, 3, 4, 5, 7, 10, 15, 20, 30
	III	0, 1, 2, 3, 4, 5, 7, 10, 15
Li (cm)	I	0, 37, 115, 165, 255, 305, 383, 420
	II	0, 35, 85, 125, 175, 210
	III	0, 11, 39, 66, 94, 105

3 EXPERIMENTAL RESULTS AND EVALUATION

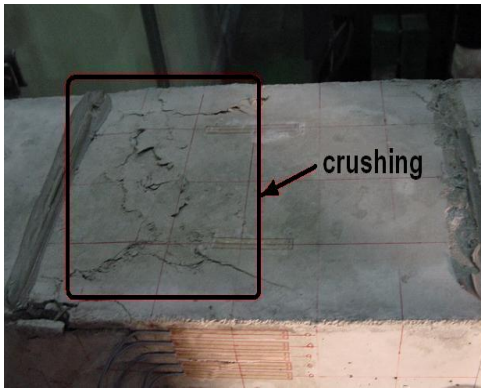
3.1 Test results

σ_N , P_u , $\epsilon_{u,test}$, and $\epsilon_{u,anal}$ represent the nominal flexural compressive strength, maximum load,

ultimate strain obtained from experiments at failure, and ultimate strain obtained from analyses at failure, correspondingly. In Equation 1, the strength in concrete σ_N is the maximum stress value in the stress-strain curve. All specimens were tested successfully where stable failure occurred in the middle section of specimens as shown in Figure 3.



(a) Side surface



(b) Top surface

Figure 3. Crack patterns of a specimen (II-2) after testing.

In Table 5, $\varepsilon_{u, test}$ is neither ultimate strain value nor the corresponding strain value at the maximum stress, but it is a reasonable maximum strain value measured using the strain gages located in the extreme compression fiber. The reason for using this strain value is due to the fact that an accurate strain cannot be obtained in the descending branch of stress-strain relationship when the failure starts in the fiber of concrete beams (i.e., beyond the maximum stress). In addition, $\varepsilon_{u, anal}$ is the strain value obtained analytically when the cross-section has a maximum bending moment value in the stress-strain relationship.

During testing, cracks in the central section (i.e., a region without shear reinforcements for all specimens occurred after formation of diagonal

tensile cracks in the parts located between supports and loading points. Finally, as shown in Figure 3, the failure occurred in the extreme compression fiber of central section with crushing preceding the failure. During testing, concrete showed more brittle failure mechanism as the specimen size increased. This is related to quasibrittle characteristics of concrete materials, energy release rate accumulated in the experimental device, and stiffness of the testing device.

3.2 Size effect of flexural compressive strength

Figure 4 shows the value $\sigma_N(d)/f_c'$ as a function of the effective depth d , the distance from the extreme compression fiber to the centroid of the steel section. In order to obtain an analytical equation, which predicts the flexural compressive strength of specimens, SEL and MSEL are used. Then, Least Square Method (LSM) regression analyses^{14,15} are performed on the results of the 6 tested specimens in this study. Equations 2 and 3 are obtained from the analyses and the results are graphed and shown in Figure 4. In this figure, the correlation coefficient (r) and standard deviation (s) for MSEL are 0.978 and 0.017 and for SEL are 0.975 and 0.018, respectively.

$$\sigma_N(d) = \frac{0.83f_c'}{\sqrt{1 + \frac{d}{4.0}}} + 0.79f_c' \quad \text{(MSEL, this study's data)} \quad (2)$$

$$\sigma_N(d) = \frac{1.25f_c'}{\sqrt{1 + \frac{d}{100}}} \quad \text{(SEL, this study's data)} \quad (3)$$

where, nominal flexural compressive strength σ_N and uniaxial compressive strength f_c' are in MPa and effective depth of the specimen d is in cm.

In this study, we also concluded that the strength ratio approaches a limit with an increasing effective depth d . In this figure, the solid circular data points represent experimental data of this study. In addition, the thick solid line and the dashed line represent the results from Equations 2 and 3, respectively.

As shown in Figure 4, the results indicate a strong size effect condition. By comparing Equations 2 and 3, it can be seen that the difference is not apparent in the region which contains most

of the beam sizes. But, beyond this region, more specifically larger specimen sizes, the new equation (Eq. (2)) better agrees with the experimental results. Also, MSEL predicts the behavior of specimens having no initial crack or notch more appropriately. If specimens have initial cracks, however, Equation 3 is better than Equation 2, because the strength decreases continuously as the specimen size increases.

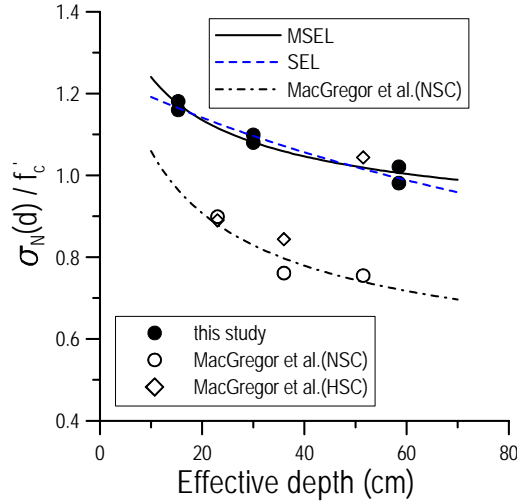


Figure 4. Relationship between $\sigma_N(d)/f'_c$ and effective depth.

In Figure 4, the hollow circular data points and the diamond-shape data points represent experimental data of normal-strength (NSC) and high strength-concrete (HSC), respectively, from the reports by Alca, Alexander, and MacGregor.¹⁶ Corley¹⁷ and Alca, Alexander, and MacGregor¹⁶ rejected the hypothesis that there is a size effect in flexure based on the experimental results. From this figure, however, the authors acknowledged that there is a little evidence of existence of size effect in flexural member, which is supported by the results from this study. In this figure, the one dotted line represents the results from Equation 4 for NSC.

$$\sigma_N(d) = \frac{1.20f'_c}{\sqrt{1 + \frac{d}{4.0}}} + 0.42f'_c$$

(MSEL, MacGregor et al.'s data) (4)

From the few available experimental data, it is also apparent that the flexural strength decreases as specimen size increases.

3.3 Comparison of proposed and existing model equations based on depth of neutral axis

Figure 5 shows the value $\sigma_N(c)/f'_c$ as a function of the neutral axis depth c , the distance from the extreme compression fiber to the neutral axis. Equations 5 and 6 are also obtained from the LSM regression analyses on the test data for neutral axis depth. Figure 5 is a graph of the results obtained from this study.

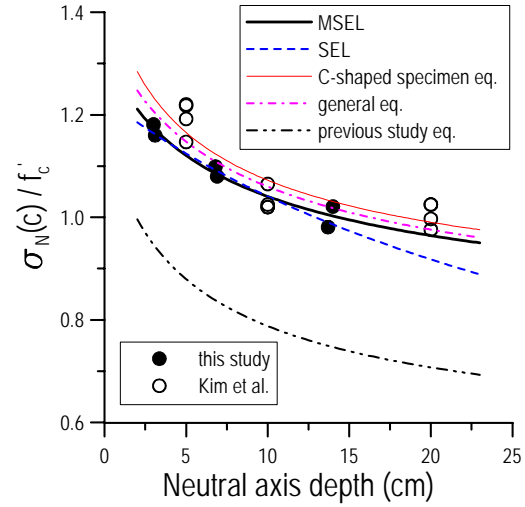


Figure 5. Relationship between $\sigma_N(c)/f'_c$ and depth to neutral axis.

$$\sigma_N(c) = \frac{0.60f'_c}{\sqrt{1 + \frac{c}{4.0}}} + 0.72f'_c$$

(MSEL, this study's data) (5)

$$\sigma_N(c) = \frac{1.23f'_c}{\sqrt{1 + \frac{c}{25.0}}}$$

(SEL, this study's data) (6)

where, depth to neutral axis of beam specimen c is in cm.

Equations 7 and 8 are obtained from the LSM regression analyses on the test data obtained from Kim et al.'s study⁸ and a combination of Kim et al.'s study⁸ and this study, respectively. Namely, Equation 8 is a more general equation since it is derived using all of available data. The results are also graphically shown in Figure 5.

$$\sigma_N(c) = \frac{0.71f_c'}{\sqrt{1 + \frac{c}{2.60}}} + 0.75f_c' \quad (7)$$

(MSEL, Kim et al.'s data)

$$\sigma_N(c) = \frac{0.66f_c'}{\sqrt{1 + \frac{c}{4.0}}} + 0.71f_c' \quad (8)$$

(MSEL, both data)

where, c is depth of neutral axis of beam specimen or C-shaped specimen in cm. In Kim et al.'s study,⁸ the maximum aggregate size was 13 mm. Thus, $l_o = 2.0 \times d_a = 2.60$ cm was used.

In the previous study,⁸ Equation 9 was proposed to obtain the flexural compressive strength of C-shaped specimens with length-depth ratio of 2:1.

$$\sigma_N(c) = \frac{0.70f_c'}{\sqrt{1 + \frac{c}{2.60}}} + 0.47f_c' \quad (9)$$

where, depth of C-shaped specimen c is in cm.

In this figure, the solid circular data points and the hollow circular data points represent experimental data of this study and Kim et al.,⁸ respectively. In addition, the thick solid line, the dashed line, the dotted line, the one dotted line, and the two dotted line represent the results from Equations 5-9, respectively.

As shown in Figure 6, the results indicate a strong size effect condition. The comparison of Equations 5-8 show that the shape and trend is similar even though a slight scattering between curves smaller and larger specimens exist. However, the $\sigma_N(c)/f_c'$ value of beam specimens is smaller than the value of C-shaped specimens. Thus, an additional value must be considered to accurately obtain beam strength capacity. This difference is probably due to the method obtaining the location of neutral axis, the maximum aggregate size d_a used to obtain the experimental data, and the type of size effect law used (either SEL or MSEL). In addition, the difference between Equation 9 and others is due to the fact that the $\sigma_N(c)$ value in Equation 9 is calculated as P_u/bc . However, in other cases, $\sigma_N(c)$ means a maximum stress value in the stress-strain curve. It is also important to note that, in order to incorporate the real loading condition, the additional bending moment due to eccentricity should be considered in Equation 9.

3.4 Other observations

3.4.1 Location of neutral axis

Figure 6a shows the value of neutral axis location to effective depth ratio as a function of the normalized strain. In this figure, it is important to note that the location of neutral axis with an increasing strain goes up to extreme compression fiber for all size specimens. Also, even though the difference with specimen size is not apparent, the neutral axis is located slightly higher in smaller-size specimens when strain is greater than 0.002. This means that the flexural compressive strength at failure increases as the specimen size decreases.

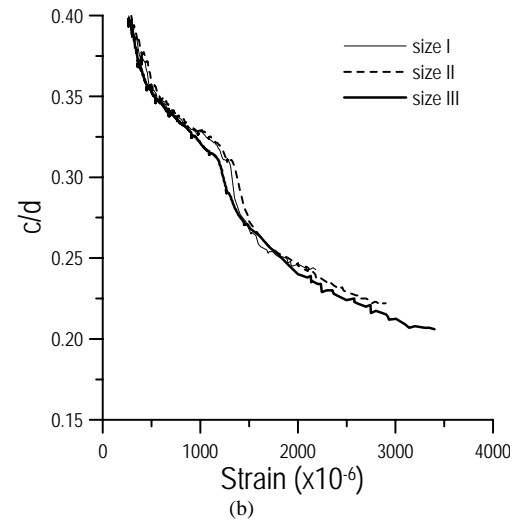
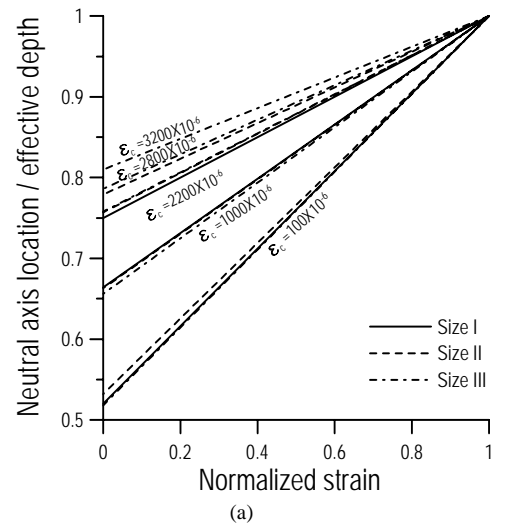


Figure 6. Variations of neutral axis location with strain in the extreme compression fiber.

Figure 6b indicates that the location of neutral axis abruptly changes when the specimens are applied with extreme compression fiber strain of $0.0012 \sim 0.0015$. This phenomenon, as shown in Figure 7, occurs on the specimens that lie in the strain range of perfect plastic behavior after tensile reinforcement yielding. This is because the flexural compressive strength increases as the strain increases even though the increase in tensile force is scarce. Accordingly, it is found that the location of neutral axis abruptly rises to satisfy the equilibrium condition between compressive and tensile forces.

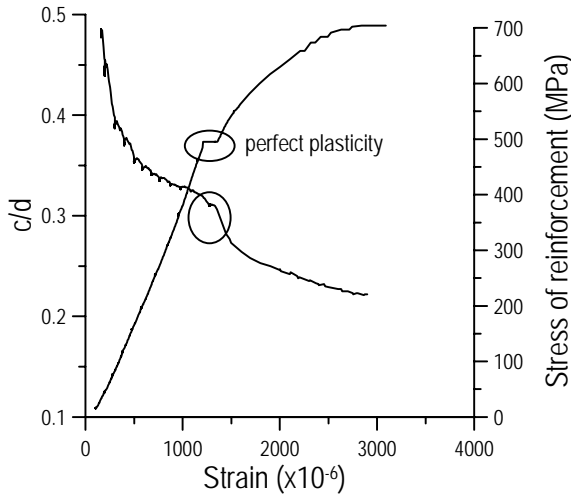


Figure 7. Variations of neutral axis location due to perfect plasticity of reinforcement with strain.

3.4.2 Stress-strain relationship

To obtain the stress-strain curve, the extreme compression fiber strain and the location of neutral axis must be compatible. However, when the specimens reach $\varepsilon_{u, test}$ it is difficult to measure strain and neutral axis location. Therefore, the strain shall be obtained from the curvature calculated using moment-displacement relationship. At this time, linear elastic mechanics theory cannot be used, because the deflection of beam is very large. Therefore, the following curvature equation was used.

$$\kappa = \frac{1}{\rho} = \frac{\nu''}{[1 + (\nu')^2]^{3/2}} \quad (10)$$

where, ν is the deflection of the beam when compared to its initial position. For deflections, a cubic $f_c = A_1 + A_2\varepsilon_c + A_3\varepsilon_c^2 + A_4\varepsilon_c^3$ equation data fitted with LSM regression analyses using

deflections measured from LVDT's shown in Figure 2b was used.

The experimentally obtained neutral axis location with respect to strain shown in Figure 6b abruptly changes when strain reaches $\varepsilon_{u, test}$. The stress-strain relationship calculated using a cubic equation was obtained by incrementally changing neutral axis depth. The final stress-strain relationship was calculated until the experimentally obtained stress-strain curve of the strain equal to $\varepsilon_{u, test}$ where the neutral axis location no longer changes. When comparing the calculated and experimentally obtained stress-strain relationships, the difference was not apparent in the ascending branch and an insignificant difference was found in the descending branch. Therefore, it is safe to conclude that in all strain states the calculated stress-strain relationship is valid and similar to the actual beam stress-strain relationship.

The depth of neutral axis has direct relationship to extreme fiber strain of flexural loaded beam members. Stress values on compressed face of specimens f_c obtained from LSM regression analyses using a cubic equation are plotted with respect to strain values on compressed face ε_c in Figure 8. LSM regression analysis was performed on the experimental data by satisfying moment equilibrium around the neutral axis of the cross-section. In other words, in order to perform LSM regression, the values of bending moment M and extreme compression fiber strain ε_c at every loading step are required. Averaged values from two stress-strain curves are plotted with respect to specimen size in Figure 8. This figure shows generally expected stress-strain relationship.

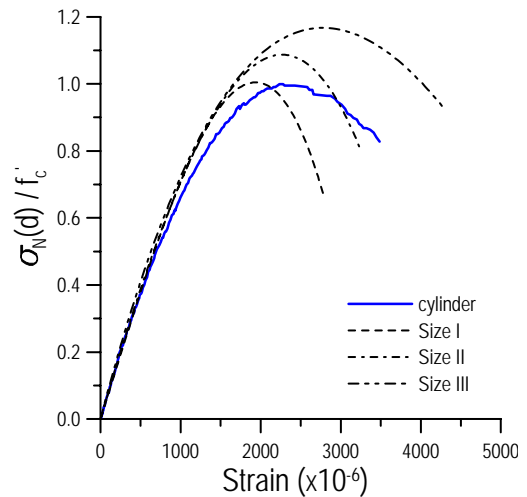


Figure 8. Effect of specimen sizes on stress-strain curves.

The thick solid line in Figure 8 is the uniaxial compressive stress-strain curve obtained from standard concrete cylinder tests. Maximum stress value and the corresponding strain value and the ultimate strain value of beam specimens show a significant increase as the specimen size decreases. The maximum stress value and the corresponding strain value of specimen size III is largest when compared to the other specimen sizes. The stress-strain curves from pure compression of cylindrical specimens and flexure-compression tests of RC beam specimens are similar until the maximum compressive strength f_c' is reached. However, the relationship is significantly different after the peak load. This means that the maximum stress value and the corresponding strain value of beam specimen increases and more ductile behavior occurs as the specimen size decreases.

It is assumed that the established f_c' and ϵ_c relationship is valid for all layers in the cross-section. Thus, a compressive stress can be determined from this relationship using the measured strain value.

4 CONCLUSIONS

To evaluate the size effect on the flexural compressive strength of RC flexural members considering the depth of neutral axis, a series of flexural tests for 6 concrete beam specimens and cylinders cast from the same batch with compressive strength of 37 MPa were carried out. From the test results and analyses, the following conclusions are drawn:

- (1) Size effect is apparent where the flexural compressive strength at failure and the corresponding strain value and the ultimate strain decrease as the specimen size increases. For the stress-strain relationship, the size effect is also apparent.
- (2) New parameter values of MSEL are suggested to better predict the reduction phenomena of the strength.
- (3) Further experimental study is needed to evaluate ultimate strain and depth of the equivalent rectangular stress block suggested in design code for RC beams. Additionally, the technical review on a mechanical relationship between RC beam specimens and C-shaped specimens will be performed.

5 ACKNOWLEDGMENT

This research was supported by the National Research Laboratory program from Ministry of Science and Technology of Korea for development of cracking control technique of concrete structure. This support is deeply appreciated.

6 REFERENCES

- ACI Committee 318-02. 2002. Building Code Requirements for Structural Concrete (ACI 318-02) and Commentary (ACI 318R-02). American Concrete Institute, Farmington Hills, Michigan, 443pp.
- Alca, N., Alexander, S.D.B., & MacGregor, J.G. 1997. Effect of Size on Flexural Behavior of High-Strength Concrete Beams. *ACI Structural Journal* 94(1): 59-67.
- Bazant, Z.P. 1984. Size Effect in Blunt Fracture; Concrete, Rock Metal. *Journal of Engineering Mechanics, ASCE* 110(4): 518-535.
- Bazant, Z.P. 1989. Identification of Strain-Softening Constitutive Relation from Uniaxial Tests by Series Coupling Model for Localization. *Cement and Concrete Research* 19: 973-977.
- Benjamin, J.R. & Cornell, C.A. 1970. *Probability, Statistics, and Decision for Civil Engineers*. McGraw-Hill, New York, Section 4.3.
- Corley, G.W. 1966. Rotational Capacity of Reinforced Concrete Beams. *Proceedings, ASCE* 92(ST5): 121-146.
- Gonnerman, H.F. 1925. Effect of Size and Shape of Test Specimen on Compressive Strength of Concrete. *ASTM, Proceedings* 25: 237-250.
- Hillerborg, A. 1988. Fracture Mechanics Concepts Applied to Moment Capacity and Rotational Capacity of Reinforced Beams. *Proceedings, International Conference on Fracture and Damage Mechanics of Concrete and Rock, Vienna*, 233-240.
- Hognestad, E., Hanson, N.W., & McHenry, D. 1955. Concrete Stress Distribution in Ultimate Strength Design. *ACI Journal* 27(4) (Proceedings V.52): 455-479, also PCA Development Bulletin D6.
- IMSL, Library, Edition 8, IMSL, Inc.
- Kaar, P.H., Hanson, N.W., & Capell, H.T. 1977. Stress-Strain Characteristics of High-Strength Concrete. *PCA Research and Development Bulletin* RD051.01D, 1-10.
- Kim, J.K., Eo, S.H., & Park, H.K. 1989. Size Effect in Concrete Structures without Initial Crack. *Fracture Mechanics: Application to Concrete, SP-118, ACI, Detroit*, 179-196.
- Kim, J.K. & Eo, S.H. 1990. Size Effect in Concrete Specimens with Dissimilar Initial Cracks. *Magazine Concrete Research* 42(153): 233-238.
- Kim, J.K., Yi, S.T., Park, C.K., & Eo, S.H. 1999. Size Effect on Compressive Strength of Plain and Spirally Reinforced Concrete Cylinders. *ACI Structural Journal* 96(1): 88-94.
- Kim, J.K., Yi, S.T., & Yang, E.I. 2000. Size Effect on Flexural Compressive Strength of Concrete Specimens. *ACI Structural Journal* 97(2): 291-296.
- Kim, J.K., Yi, S.T., & Kim, J.H.J. 2001. Effect of Specimen Sizes on Flexural Compressive Strength of Concrete. *ACI Structural Journal* 98(3): 416-424.
- Yi, S.T., Kim, J.H.J., & Kim, J.K. 2002. Effect of Specimen Sizes on ACI Rectangular Stress Block for Concrete Flexural Members. *ACI Structural Journal* 99(5): 701-708.